REVIEW ARTICLE

Precise orbit determination for the Haiyang-2D satellite using new onboard BDS-3 B1C/B2a signal measurements

Min Li[1] · Renhai Mu[1] · Kecai Jiang[1] · Youcun Wang[1] · Xuanxuan Zhang[2] · Chuntao Chang[2] · Qile Zhao[1]

Abstract

The GNSS receiver onboard the Haiyang-2D (HY-2D) China Ocean satellite tracks the new B1C and B2a signals of BDS-3 to orbit determination. This study analyzes one week of onboard dual-frequency BDS-3 data obtained during July 2021 from the HY-2D satellite. The quality of the onboard BDS-3 measurements is first evaluated in terms of the data quantity and code multipath error quantities. Thanks to the IGSO and GEO satellites of BDS-3, the HY-2D satellite can observe more BDS-3 satellites in China and surrounding areas. The multipath errors (MPs) of the B1C and B2a signals are approximately 0.6 m and 0.2 m, respectively; they have centimeter-level systematic biases which change linearly with elevation. For precise orbit determination (POD), the observable-specific signal biases (OSBs) are corrected by the OSB products obtained from the GNSS Research Center of Wuhan University (WHU), showing that the ionospheric-free code residuals of B1C and B2a signals are reduced from 5.6 to 1.3 m. The phase center variation (PCV) model is corrected by the residual approach, and the orbit determination residuals of carrier phases can be improved to 7.5 mm. The orbit accuracy, indicated by the satellite laser ranging (SLR) validation, is about 2.3 cm during the study period. Upon conducting the Doppler Orbitography and Radio-positioning Integrated by Satellite (DORIS) validation, orbit differences less than 5.2 cm in the 3D direction are obtained with the BDS-3-based orbits, and high consistency is achieved in the radial orbit component.

Keywords HY-2D · BDS-3 · B1C/B2a signals · Data quality · Precise orbit determination

Introduction

The Haiyang-2D (HY-2D) marine dynamic environment satellite was launched by the National Satellite Ocean Application Service (NSOAS) on May 19, 2021. Its purpose is to measure the height, wind, and temperature of the sea surface (NSOAS 2022). The analysis of altimeter data relies on precise orbit position with high accuracy, requiring 3D root-mean-square (RMS) orbit errors of less than 5 cm, which makes precise orbit determination (POD) particularly challenging. In the past two decades, much research has been carried out using the onboard Global Navigation Satellite System (GNSS) technique, which has reached orbit accuracy at the centimeter level (Bock et al. 2002; Kang et al.

2003; Kroes et al. 2005; Montenbruck et al. 2018). Bock et al. (2007) corrected several error sources of the Gravity field and steady-state Ocean Circulation Explorer (GOCE) of the European Space Agency (ESA), and the accuracy of the orbit was better than 2 cm when fixing ambiguities. 2009) used the double−difference. Regarding the Gravity Recovery and Climate Experiment (GRACE) satellites of the USA, Jäggi et al. (2009) used the double−differencereduced dynamic baseline methods to achieve an orbital accuracy of better than 5 cm in each direction Van et al. (2013) analyzed POD results from several institutions of the Challenging Minisatellite Payload (CHAMP) satellites, and the results showed that the orbit overlap accuracy was less than 4.5 cm in the 3D direction. Montenbruck et al. (2021) achieved orbit accuracy of better than 1.5 cm in terms of height errors based on GPS and Galileo tracking, and the RMS consistency between the Satellite Laser Ranging (SLR) normal points and the precise orbits was better than 1 cm. Peng et al. (2021) fixed the single-difference ambiguity when conducting POD for the HY-2B satellite, and the accuracy was improved by 1–3 mm during the POD analysis

✉ Min Li
limin@whu.edu.cn

[1] GNSS Research Center, Wuhan University, 129 Luoyu Road, Wuhan 430079, China

[2] Chinese Academy of Surveying & Mapping, Beijing, 100036, China

and SLR validation. Wang et al. (2022) developed a mathematical description of the yaw model to account for the attitude mode of the HY-2C satellite by using onboard GPS observations. According to the orbit assessment results, the orbit self-consistencies of 0.43 cm and 1.46 cm were reached in the radial and 3D RMS of the overlapping difference, respectively.

As in other GNSS systems, such as BDS, the data quality and precise position performance achieved by using the global Multi-GNSS experiment (MGEX) and International GNSS Monitoring & Assessment System (iGMAS) ground station observations are of great interest to the geodesy community (Jiao et al. 2011; Montenbruck et al. 2017; Shi et al. 2021). As for data observation quality, the carrier-to-noise ratio (C/N) of the B2a signal is greater than that of the B1C, B1I, and B3I signals by approximately 4.0 dB. Compared with other signals, the B2a signal has the strongest anti-multipath ability, for which multipath error (MP) is approximately 0.3 m (Hauschild et al. 2012; Mu et al. 2020). Regarding precise positioning, Odijk et al. (2015) achieved precise point positioning (PPP) via a combination of both GPS and BDS, and the convergence time was tremendously reduced to 30 min on average. Wang et al. (2021) evaluated the positioning performance for B1C and B2a signals and achieved static PPP with 2.8 cm and kinematic PPP with 10.7 cm. Overall, the studies of B1C and B2a signals have mainly focused on ground applications. However, the signal quality and the POD performance for space applications are still not clear and need further investigation.

Several studies have already been performed using the onboard BDS observations to investigate the POD precision of low earth orbit (LEO) satellites (Zhao et al. 2017; Li et al. 2019). Li et al. (2017) achieved the orbit overlap accuracy of better than 2 cm for the POD of the Fengyun-3C satellite by using the onboard BDS-2 and GPS observations; the orbit difference in terms of 3D RMS, compared with GPS-derived ones, is 0.75 cm. Zhao et al. (2017) used the FY3C onboard BDS-2 data to determine the dynamic orbits; the 3D RMS of orbit differences between GPS-only solutions and Bei-Dou-only solutions is about 15.8 cm. Li et al. (2019) jointly processed the BDS-2/GPS observations of ground stations and two FY-3 satellites in a least-squares adjustment, which made a high level of consistency, and the corresponding precision improvement can reach 25% for the GPS and BDS-2 POD. Zhao et al. (2020) studied the onboard B1I/B3I of BDS-2/3 observations of the Tianping-1B satellite, and the SLR residual RMS was less than 2.5 cm. These results show that methods utilizing onboard B1I and B3I signal data from BDS can achieve the same level of accuracy as GPS.

The recently launched HY-2D satellite can receive the B1C/B2a dual-frequency signals of the BDS-3. Compared with the old signals of BDS-2, the new B1C and B2a signals can promote the compatibility as well as interoperability between BDS-3 and GNSS (Yang et al. 2020), as shown in Table 1 (CSNO 2021). Due to the successful networking of the BDS-3 system, orbit determination for LEO satellites with BDS-3 signals, especially new frequency signals, will become mainstream in China. Since the BDS-3 satellite constellation was built, the current 24 medium earth orbit (MEO) satellites (C19–C30, C32–C37, C41–C46) and 3 Inclined geosynchronous orbit (IGSO) satellites (C38–C40) are capable of broadcasting the B1C and B2a frequencies (CSNO 2021) have been launched. Fortunately, the HY-2D satellite can receive the two new frequencies of these BDS-3 satellites, and thus, the analysis of the onboard data quality and orbit precision of these signals is of great reference value for the application of BDS-3 in the orbit determination of LEO satellites. Therefore, based on HY-2D tracking data, this paper analyzes the new frequency signals onboard BDS-3 in detail.

Given this background, we mainly study the performance and contribution of the new dual-frequency (B1C and B2a) signals of the BDS-3 to LEO satellite POD. First, we introduce the HY-2D platform, collect one week of data from July

Table 1 Frequency and wavelength of the BDS-3/GNSS system (CSNO 2021)

Navigation system	Channel	Reference frequency/MHz	Code rate/Mcps	Expansion factor	Standard frequency/MHz	Wavelength/m
BDS-2/3	B1I	2.046	2.046	763	1561.098	0.1920
	B3I	2.046	10.23	620	1268.520	0.2363
BDS-3	B1C	2.046	1.023	770	1575.420	0.1903
	B2a	2.046	10.23	575	1176.450	0.2548
GPS	L1	1.023	1.023	1540	1575.420	0.1903
	L2	1.023	10.23	1200	1227.600	0.2442
	L5	1.023	10.23	1150	1176.450	0.2548
GALILEO	E1	1.023	1.023	1540	1575.420	0.1903
	E5a	1.023	10.23	1150	1176.450	0.2548
	E5b	1.023	10.23	1180	1207.140	0.2483

2021, and evaluate the observation quality of the onboard BDS-3 receiver regarding data availability and multipath errors. After that, we focus on the methods and strategies of orbital parameter estimation. Then, we validate the POD accuracy of the new frequencies of BDS-3 satellites with the HY-2D satellite by using various forms of self-consistency tests and external validation with SLR measurements and Doppler Orbitography and Radio-positioning Integrated by Satellite (DORIS) orbits. Finally, a discussion and conclusions are summarized.

Haiyang-2D POD package and experimental data

The HY-2D satellite carries several scientific instruments, including a microwave imager to collect information for disaster and weather forecasting, a radar altimeter used to measure the distance from the satellite to the sea surface, and a radar scatterometer for measuring the sea surface wind field (NSOAS 2022). These instruments are deemed necessary with positioning requirements in the meter to centimeter range. To achieve this target requirement, the HY-2D satellite is equipped with GNSS receivers, laser retroreflector array (LRA), and DORIS. Figure 1 shows the picture of the HY-2D satellite. The orbital inclination is 66°, the regression period is 10 days, and the orbital height at the end of the life is 958.490 km (NSOAS 2022). From the information provided by NSOAS, when the HY-2D satellite is in normal orbit, to provide continuous energy, the satellite performs a continuous attitude yaw mode operation.

The HY-2D satellite is equipped with two GNSS receivers as its key tracking system and records the observed code and carrier phase observations. The first GNSS receiver serves as the main equipment but only receives GPS signals, and the second receiver is a backup device that can receive BDS-3 new signals. However, the backup BDS-3 receiver was switched on during the in-orbit testing phase for a period of time. Fortunately, we collect BDS-3 observations from July 7–13 (DOY 188–194), 2021, at

30-s intervals. These valuable BDS-3 observations can provide opportunities for investigating the quality of the onboard data as well as the POD performances achieved by using these data.

As for the satellite coordinate system, the satellite body-fixed (SBF) frame of the HY-2D spacecraft is defined as follows: the center of mass (COM) is defined as the origin of the SBF frame, the $+X$-axis points along the satellite velocity direction, and the $+Z$-axis points toward the earth's surface, while the Y-axis completes a right-hand coordinate system with $Z = X \times Y$. As provided by NSOAS, the phase center offset (PCO) of the positioning antenna (PA) is measured as $(0.427, 0.178, -1.379)$ m for the B1C signal and $(0.428, 0.178, -1.406)$ m for the B2a signal, relative to the COM in the SBF frame.

Data availability

As the POD calculations utilize the undifferenced, ionosphere-free carrier phase and code linear combination as basic observation equations, both the code and carrier phase observations from the new frequencies of BDS-3 are needed during each epoch. The number of observed BDS-3 satellites per epoch along the HY-2D ground tracks is shown in Fig. 2. Figure 3 shows the mean percentage of the number of BDS-3 satellites received from DOY 188 to 194 in 2021. As the BDS-3 has been completed in 2020, it can receive more than four satellites with 93% of the time for the HY-2D onboard GNSS receiver. However, the HY-2D satellite can only receive 4 to 6 BDS-3 satellites in most periods, mainly because the BDS-3 has a total of 24 MEO satellites, fewer than GPS. Among them, thanks to the 3 IGSO and 3 GEO satellites of BDS-3, the number of satellite observations on the sea surface around China is higher than that in other areas, and more than 7 satellites can be observed by the HY-2D satellite.
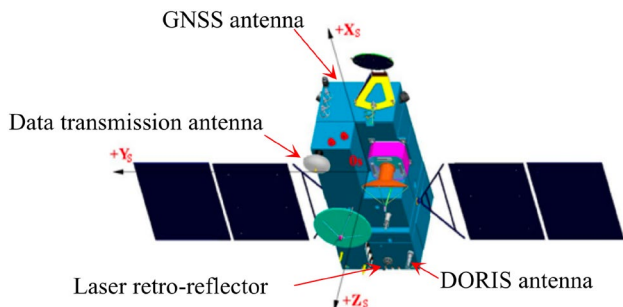

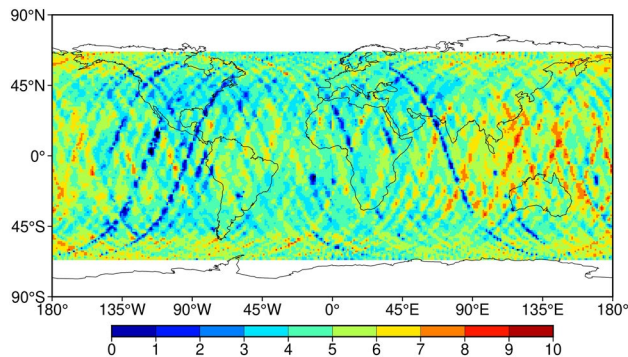**Fig. 1** Visualization of the HY-2D satellite

Fig. 2 Numbers of observed BDS-3 satellites per epoch along the HY-2D satellite ground tracks from DOY 188 to 194 in 2021. Different colors indicate the different number of satellites
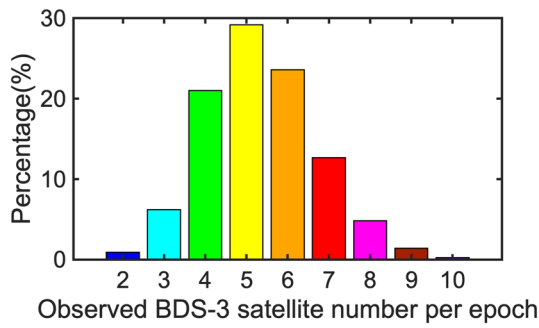
Fig. 3 Data availability statistics for the HY-2D satellite. Different color bars indicate the percentages of different numbers of satellite observations
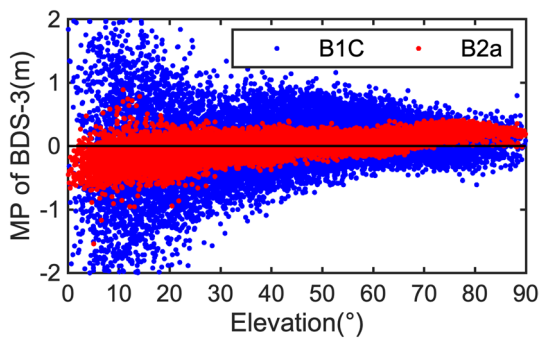

Fig. 4 MP variations with the elevation of the B1C and B2a signals for all BDS-3 satellites. Note that the blue dots represent the variations in MP1 over time and elevation, and the red dots represent the MP2 variations

Code multipath errors

The onboard BDS-3 code multipath errors are calculated by using multipath combinations with dual-frequency code and carrier phase observations (Tranquilla et al. 1990; Rocken et al. 1992; Breivik et al. 1997). Figure 4 shows the variations of the MPs of B1C and B2a signals against the elevation for all BDS-3 satellites on DOY 191. The MPs of the B1C signal (MP1) at low elevation angles are affected more severely and are approximately 1.0 m with an elevation below 60°. The MPs of the B2a signal (MP2) exhibit a much smaller variation than MP1, which generally are less than 0.5 m, and the MPs have a strong correlation with SNR, showing the same frequency and in-phase characteristics (Bilich et al. 2007a; Bilich et al. 2007b). However, it can be seen that the MPs of B1C and B2a signals are unevenly distributed above and below zero. The systematic biases, linearly depending on elevation, are small: 0.02 m and 0.06 m for B1C and B2a signals, respectively. These systematic biases may be related to the incident direction of the signals (Montenbruck et al. 2008).

Figure 5 shows the RMS statistics of the MPs for the B1C and B2a frequencies in DOY 188 to 194. The MP RMS of B1C and B2a are approximately 0.58 m and 0.19 m, respectively. Compared with the B1C signal of BDS-3, the B2a signal has strong multipath resistance (Lu et al. 2019; Montenbruck et al. 2020). According to Table 1, the clip rate of the B1C and B2a signals of BDS-3 is 1.023 Mcps and 10.23 Mcps, respectively. The higher code chip rate can improve the code resolution and help the receiver to reduce the error level when capturing the signals (Enge 2003).

POD by utilizing onboard BDS-3 B1C/B2a measurements

In this study, we mainly analyze the performance of the BDS-3/GNSS-based POD approach for the HY-2D satellite by using the Position And Navigation Data Analyst (PANDA) software developed by the GNSS Center of Wuhan University, as this approach is widely used for LEO satellite POD (Zhao 2004).

Fig. 5 RMS of the MPs for B1C and B2a signals of the HY-2D satellite. The blue and red bars represent the MP RMS of B1C and B2a signals, respectively
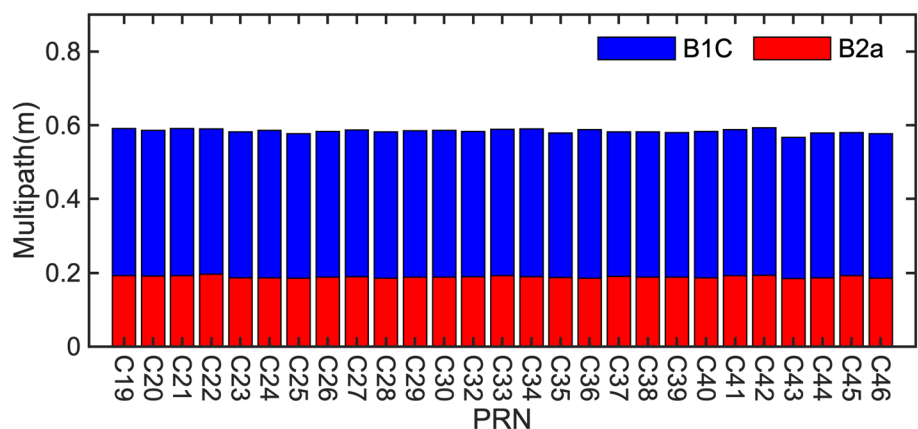
POD strategy

The information regarding the employed dynamical model, the parameter sets, and the reference system conventions are summarized in Table 2. Both static field and time-varying gravity are calculated by the state-of-the-art EIGEN-06C earth gravity model (Shako et al. 2014) truncated to the degree and order of 120 and 50, respectively. The FES2004 model (Lyard et al. 2006) is used for calculating the ocean tide, while models derived from the IERS Conventions 2010 (Petit et al. 2010) are used for solid earth tide and pole tide perturbations as well as relativistic effects.

Table 3 shows the parameters for the simple box-wing model used in this work for describing non-conservative forces, including the atmospheric drag and solar radiation pressure forces. In order to compensate for the un-modeled atmospheric drag and solar radiation pressure forces, piecewise constant empirical accelerations at an interval of 120 min in the along-track direction and the cross-track direction are introduced to absorb the dynamic model errors.

Based on the above POD strategy, we first consider the existence of code biases between the satellite and receiver. The OSB corrections are performed on the code observations, and the effect of these biases on the orbit determination

Table 2 Summary of the POD strategy used for the HY-2D satellite

Analysis strategy	Description
Dynamic model	
Gravity model	EIGEN-06C, up to degree and order 120
Conventional inertial reference frame	J2000.0
Precession and nutation	IERS 2010 (Petit and Luzum 2010)
Earth orientation	IERS C-04 (Gambis 2004)
Solid earth tide and pole tide	IERS 2010 (Petit and Luzum 2010)
Ocean tide	FES2004 30×30 (Lyard et al. 2006)
Ocean pole tides	Desai (2002)
Relativity	IERS 2010 (Luzum and Petit 2012)
Atmosphere drag	DTM 2013
Solar radiation Box-wing model	(Marshall and Luthcke 1994)
N-body perturbation	JPL DE430 (Folkner et al. 2014)
Observation model	
The observation model	IF (ionosphere-free linear combination)
Elevation cut-off angle	0°
Interval and arc length	30 s and 30 h
BDS-3 satellites antenna PCO/PCV	IGS igs14.atx antenna model (week 2163)
BDS-3 ephemeris and clock	BDS-3 products provide by GFZ (30 s interval for clock products)
Estimated parameters	
Initial state	Position and velocity at the initial epoch
Receiver clock offset	Epoch-wise clock offsets
Phase ambiguities	Each continuous tracking arc as a float
Solar radiation coefficients	One per 30 h arc
Drag coefficients	One per 120 min
Empirical coefficients	One per 120 min; amplitudes of periodic empirical accelerations acting in the along-track and cross-track directions

Table 3 HY-2D satellite macro-model (NSOAS 2022)

Element	Areas (m²)	Visible			Infra-red		
		Specular	Diffuse	Absorbed	Specular	Diffuse	Absorbed
Body+X	3.621	0.650	0.000	0.350	0.000	0.310	0.690
Body−X	3.920	0.650	0.000	0.350	0.000	0.310	0.690
Body+Y	5.173	0.650	0.000	0.350	0.000	0.310	0.690
Body−Y	5.461	0.650	0.000	0.350	0.000	0.310	0.690
Body+Z	3.060	0.650	0.000	0.350	0.000	0.310	0.690
Body−Z	6.224	0.650	0.000	0.350	0.000	0.310	0.690

code residuals is evaluated. Next, we use the 7-day (DOY 188–194) onboard observations of the HY-2D satellite to analyze the POD results with antenna phase center variation (PCV) corrections. Finally, the orbit determination solution is determined by the above correction method, and the LEO satellite orbit arc length is set for 30 continuous hours over a single day (from 21:00 on the previous day to 3:00 on the next day).

Pseudorange observation bias corrections

In this study, we use the BDS-3 precise orbit and clock products provided by GFZ (Helmholtz-Centre Potsdam-German Research Centre for Geosciences) to perform orbit determination for the HY-2D satellite. However, these products are aligned with B1I and B3I frequency references (Männel et al. 2017; Montenbruck et al. 2017), so bias occurs when utilizing B1C and B2a signals for POD. In the GNSS community, there are different ways to cope with these biases, such as differential code bias (DCB) corrections (Sanz et al. 2017) or observable-specific signal bias (OSB) corrections (Villiger et al. 2019). Compared to the traditional DCBs, OSBs are more flexible for dealing with multi-GNSS code biases, and each specific observable type has an individual delay. Thus, OSBs are straightforward in terms of their application (Villiger et al. 2019). Currently, OSB products are generated by the GNSS Research Center of Wuhan University (WHU). Deng et al. (2021) estimated the OSBs of BDS-2/3 and found that the OSB estimates of BDS-3 exhibited better stability than the BDS-2 OSBs.

Figure 6 lists the bias time series of the B1C and B2a frequencies for each BDS-3 satellite released by WHU from DOY 188 to 194. It can be seen that the OSB for each signal of the BDS-3 satellites is stable in these 7 days, but its values are different for different signals of different satellites. The degree of divergence reaches around 100 ns, the equivalent distance error reaching the range of several meters. According to Deng et al. (2021), compared with other signals of multi-GNSS such as the L1 and L2 signals of GPS, the E1, E5a, and E5b signals of Galileo, etc., the stability of BDS-3 new signals is approximately 0.3 ns worse than other system signals in the long term, but better than B1I and B3I signals of BDS-2 (Deng et al. 2021). Therefore, code biases need to be considered during orbit determination.

As shown in Fig. 6, the OSBs can cause ranging errors of several to tens of meters for each BDS-3 satellite. To eliminate the influence of the code observation biases inherent in the B1C and B2a signals on orbit determination accuracy, we use the OSB products provided by WHU to correct these biases. Figure 7 shows the residual RMS of the code before and after OSB corrections. The RMS decreases from approximately 5.6 m to approximately 1.3 m. The accuracy of the pseudorange residuals improves by over 77% for each day. As this study uses orbit and clock products based on the BDS B1I and B3I frequencies, the pseudorange residuals improvements reach several meters after performing OSB corrections. Therefore, these results indicate that it is necessary to correct the OSBs when utilizing different reference frequencies to determine high-precision orbits. Thus, the corrected observations are used for the follow-up POD study.

Fig. 6 B1C and B2a OSBs of each BDS-3 satellite from DOY 188 to 194. Different colors indicate different BDS-3 satellites
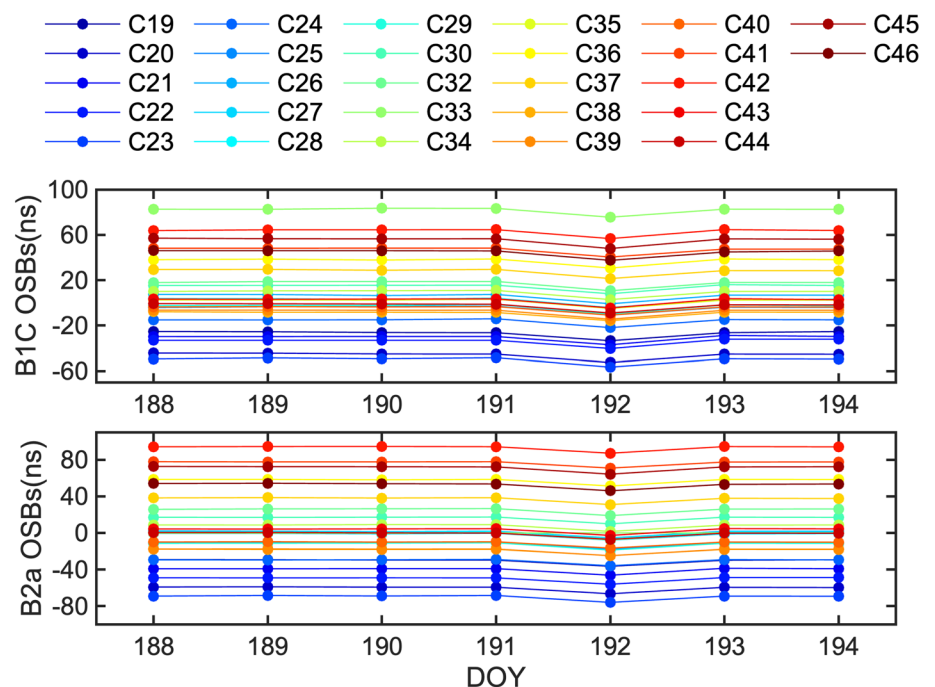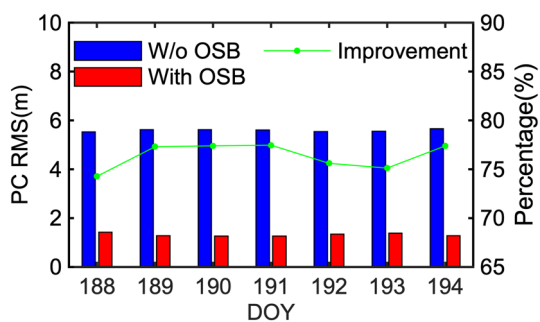
Fig. 7 PC RMS before and after performing OSB corrections from DOY 188 to 194 in 2021. The blue and red bars represent the PC residual RMS accuracies before and after using OSB products, respectively, and the green dots represent the accuracy improvement percentages
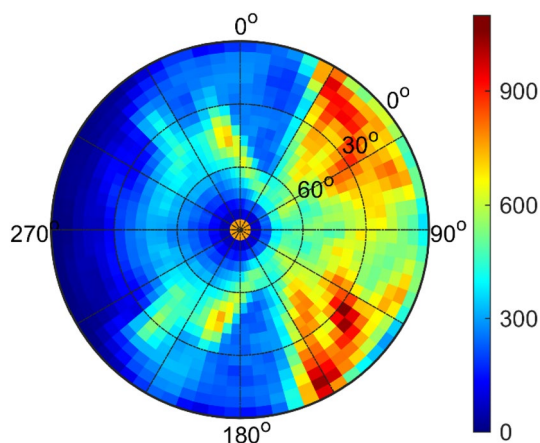

Fig. 8 Sky-plots of the total observations for 5×5° PCV correction

Phase center variation corrections

For the LEO POD, the antenna PCO and PCV must be carefully modeled. The residual stacking approach is employed to correct the PCV model, and the variations are represented as piecewise linear functions concerning the zenith and azimuth angles in the corresponding antenna-fixed coordinate system (Montenbruck et al. 2003; Dilner et al. 2006; Montenbruck et al. 2009). After iterative calculation, the obtained PCV model correction is brought back into the program for orbit determination and calculation (Haines et al. 2004; Jäggi et al. 2009).

Figure 8 shows the number of observations obtained for each grid point in the PCV model corrections process for the HY-2D satellite. The onboard BDS-3 receiver provides a large number of observations between azimuth angles of 30° and 160°, particularly at 30° to 80° and 110° to 160°, where the number of observations can exceed 700 epochs. However, there are small numbers of observations in other directions, especially at an elevation of 0° to 10°, where the numbers of observations are less than 200 epochs. These results indicate that the received signals have a certain directivity; the reason may be caused by the shielding of the receiver antenna by the satellite parts such as solar panels.

Correspondingly, we correct the PCV model by using the observations from these seven days because we think the repeatability of the observed patterns in the antenna-fixed coordinate system is very high (Jäggi et al. 2007, 2009). Based on these data, we correct the PCV model by using a residual stacking approach and generate a 5°×5° correction map after three iterations. Figure 9 shows the PCV model correction map and the carrier phase residual map based on the reduced dynamic solutions. Combined with Fig. 8, although there are fewer than 200 observations at elevation angles of 0° to 10°, there is no significant effect on the PCV model corrections. The PCV model correction results are between -12 mm and 15 mm for all directions, especially at elevation angles of 40° to 90°, where the values are within ±3 mm. For the phase variations with respect to the mean PCOs, as measured in the pre-flight calibration, the results are confined to less than ±1 mm for elevations above 10°.

Carrier phase residuals can be used to measure the consistency between the applied models and the BDS-3

Fig. 9 5°×5° PCV model correction map (left) and carrier phase residual map obtained after PCV model correction (right) for the HY-2D satellite (unit: mm)
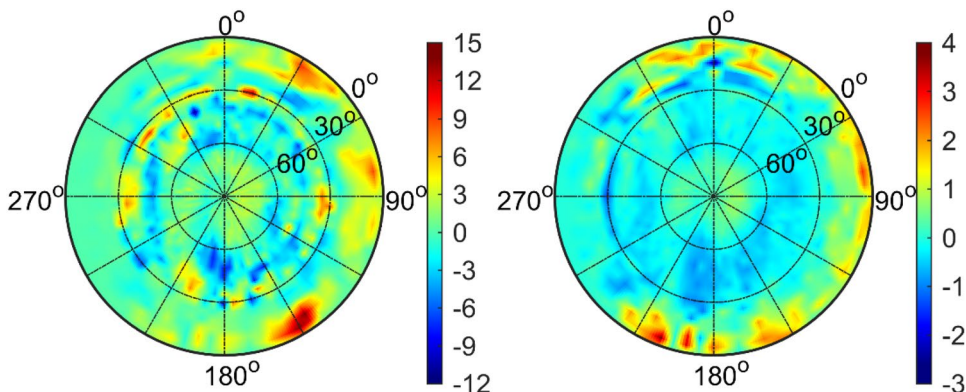
observations (Jin et al. 2021). The RMS of the carrier phase combination (LC) residuals for each day before and after conducting PCV model corrections are indicated in Fig. 10. The corrected residuals results are maintained at approximately 7.5 mm, which represents an improvement of more than 13% for each day. These results show that although the HY-2D satellite is in the continuous yaw mode, the antenna phase center variation pattern is still stable. Therefore, correcting the PCV model via the residual approach is feasible. The improved accuracy of the carrier phase residuals also underlines the importance and necessity of PCV estimation for the BDS-3 observations when conducting POD.

Orbit validation and analysis

The performance of the POD with the BDS-3 new signals is also analyzed by using SLR validation and DORIS validation. The SLR observations are provided by the

Fig. 10 LC RMS obtained before and after utilizing the PCV model corrections from DOY 188 to 194 in 2021. The blue and red bars represent the PC residual RMS accuracies before and after PCV correction, respectively, and the green dots represent the accuracy improvement percentages

International Laser Ranging Service (ILRS) (Pavlis et al. 2020), and the DORIS orbit products are provided by the Centre National d'Etudes Spatiales (CNES) (Loyer et al. 2012). These two validation methods can provide more objective accuracy evaluation results for the HY-2D orbits.

SLR validation

Independent verification of the resulting POD accuracy can be achieved through a comparison with SLR measurements (Arnold et al. 2019). Figure 11 shows that 17 ground SLR stations can observe the HY2D satellite during this period. For these global SLR stations, considering the quality and stability of the entire set of network sites over several decades, the list of core stations has been officially defined by the Analysis Working Group (Pavlis et al. 2020). Compared with basic stations, the core stations can offer normal points with precision at the 5–10 mm level (Arnold et al. 2019). Therefore, we mainly used these core stations to conduct the SLR validation.

For the above core stations, the number of SLR normal points is kept at approximately 1071 on these days. The residuals of these measurements collected until the end of DOY 194 in 2021 are shown in Fig. 12. After performing PCV model corrections, the STD of SLR residuals is reduced from 2.89 to 2.26 cm. These results demonstrate that the HY-2D satellite orbit precision is significantly improved by over 12% after performing PCV model corrections.
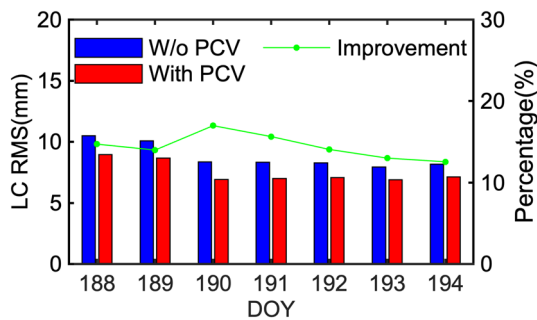
External orbit validation

The DORIS orbits provided by CNES can be used to quantify the orbit precision based on the BDS-3 solution. Comparing the two orbital products, the orbit difference results are used as the basis of the HY-2D external orbit verification.

Fig. 11 HY-2D satellite ground tracks and SLR track stations observed from DOY 188 to 194 in 2021. Different colors indicate the different DOYs. The red dots represent core stations, and the green dots represent basic stations
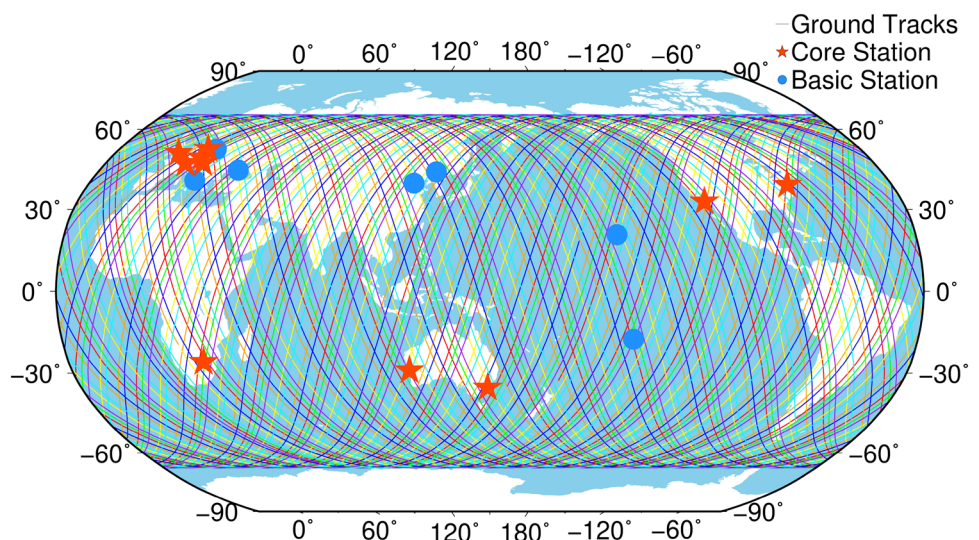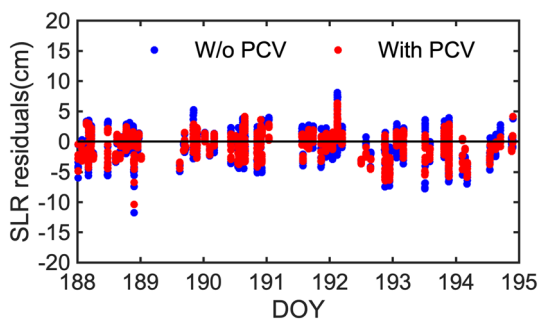
Fig. 12 Residuals of the satellite laser ranging measurements before and after performing PCO/PCV correction for the HY-2D satellite from DOY 188 to 194 in 2021. The green and red dots represent the SLR residuals obtained before and after PCV correction. The blue dots represent the SLR residuals of the HY-2D orbits using DORIS
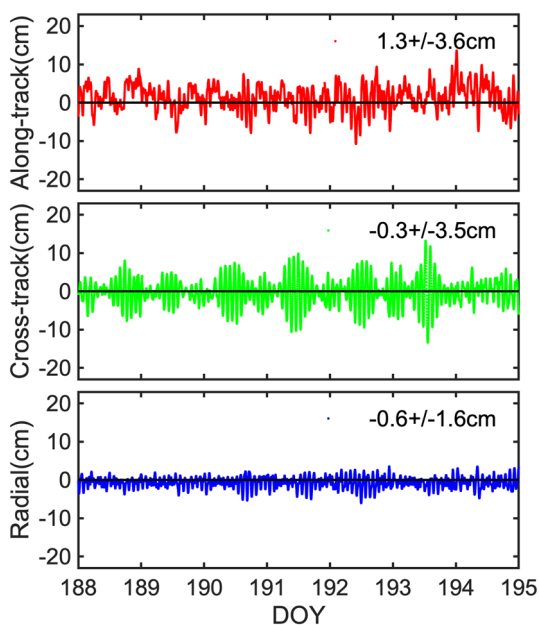

Fig. 13 Time series of the orbit differences between those obtained via DORIS and BDS-3 from DOY 188 to 194. The red, green, and blue colors indicate the orbit differences in the along-track, cross-track, and radial directions. The average and standard deviation are given in the legend

Figure 13 shows the time series of the orbit differences between DOY 188 and DOY 194. It can be seen that there is a periodic effect in the cross-track direction of orbit differences, probably due to the difference in POD strategies between GPS orbit and DORIS orbit, such as the different configuration of empirical force acceleration parameter estimation (Montenbruck et al. 2021). Moreover, the mean values of the results in the three directions are 1.3 cm, −0.3 cm, and −0.6 cm. As for the STD, the precision reaches 3.6 cm, 3.5 cm, and 1.6 cm in the three directions, and the STD of

the 3D direction reaches 5.2 cm. These results indicated that the BDS-3-based POD solution exhibits very good consistency with the DORIS results in the radial direction.

Discussion and conclusion

The HY-2D satellite is the fourth Chinese marine dynamic environment mission satellite. High-precision orbit determination is important for guaranteeing the scientific objective of the radar altimeter mission. This study analyzes B1C and B2a onboard observations obtained on the Chinese HY-2D satellite in July 2021. First, the BDS-3 observation quality is evaluated in the context of the data quantity as well as the number of code multipath errors. Following this, HY-2D POD is performed by using BDS-3 new observations, and the resulting POD precision is analyzed by code and carrier phase residual analysis, SLR validation, and DORIS validation.

Regarding the data quality assessment of the HY-2D satellite, more than four BDS-3 satellites can be received for more than 93% of the epochs, and the number of satellite observations on the sea surface around China can reach approximately seven with the addition of three IGSO satellites. Furthermore, it is worth noting that the numbers of onboard observations at azimuth angles of 30–80° and 110–160° are larger than that at other angles, which might be caused by the shielding of the receiver antenna by the satellite parts such as solar panels. The directivity may cause a slight loss of accuracy in orbit determination. Regarding the MPs, it is worth noting that there are small systematic biases depending on elevation for the B1C and B2a signals, with centimeter magnitude. Moreover, the different chip rates of observations cause multipath error differences between B2a and B1C signals. The RMS of MP1 and MP2 are approximately 0.58 m and 0.19 m, respectively. The B2a signal has stronger multipath resistance compared with the B1C signal of BDS-3.

For the POD of the HY-2D satellite with new onboard signals, OSBs need to be considered when using precise orbit and clock products based on B1I and B3I signals. After using OSB products provided by Wuhan University, the residuals of the code measurements decreased from 5.6 to 1.3 m. As for PCV model corrections, although the HY-2D satellite maintains a wide range of yaw attitude changes to keep the solar panels pointing toward the sun for energy supply purposes, a stable PCV model is still available for the onboard receiver. According to the time series results and the global SLR observation results, the residual RMS of the carrier phase decreased by more than 13%, which is less than 9 mm, and for the SLR residuals, the STD reaches 2.26 cm for the PCV model correction solution, which an improvement of over 12% for each SLR station. Compared with the DORIS orbits, the STD of the orbit differences for

the three directions is 3.6 cm, 3.5 cm, and 1.6 cm. The time series and accuracy statistics results indicate that the method utilizing the new BDS-3 signals has high consistency in the radial direction.

It is concluded that the POD precision for the HY-2D satellite when using new onboard BDS-3 signal observations can reach up to 2.0 cm in the radial direction, but it is still not as good as the GPS solutions. With the increasing data received from the ground, the continuous improvement of BDS-3 precise orbit and clock products will increase the orbit accuracy of the onboard BDS-3 observations for LEO satellites. Moreover, the ambiguity resolution based on BDS-3 observations will be helpful for the orbit accuracy improvement of LEO satellites. This study serves as a valuable reference for future onboard BDS-3/GNSS research.

Data availability The GNSS precise orbit and clock products are publicly available from ftp:// igs.gnsswhu.cn/pub/gnss/products/mgex/. The SLR observations of HY-2D are provided by ILRS at ftp://cddis.gsfc. nasa.gov/pub/slr/data/. The SLRF2014 station coordinates are obtained from ftp://gdc.cddis.eosdis.nasa. gov/pub/slr/products/resource/. The LRR offset information is available at https://ilrs.cddis.eosdis.nasa.gov/ missions/satellite_missions/current_missins/hy2d_reflector.html. The other data that support this study are available from the corresponding author upon reasonable request.

References

Arnold D, Montenbruck O, Hackel S, Sośnica K (2019) Satellite laser ranging to low earth orbiters: orbit and network validation. J Geod 93(11):2315–2334. https://doi.org/10.1007/s00190-018-1140-4

Bilich A, Larson K (2007a) Mapping the GPS multipath environment using the signal-to-noise. Radio Sci 42

Bilich A, Axelrad P, Larson K (2007b) Scientific utility of the signal-to-noise ratio (SNR) reported by geodetic gps receivers. In: Proc. ION GNSS 2007b, institute of navigation, fort worth, TX, September 2007b, pp 1999–2010

Bock H, Hugentobler U, Springer TA, Beutler G (2002) Efficient precise orbit determination of LEO satellites using GPS. Adv Space Res 30(2):295–300. https://doi.org/10.1016/S0273-1177(02)00298-3

Bock H, Jäggi A, Švehla D, Beutlera G, Hugentoblerb U, Visserc P (2007) Precise orbit determination for the GOCE satellite using GPS. Adv Space Res 39(10):1638–1647

Breivik K, Forssell B, Kee C, Enge P, Walter T (1997) Estimation of multipath error in GPS pseudorange measurements. Navigation 44(1):43–52. https://doi.org/10.1002/j.2161-4296.1997.tb01938.x

China Satellite Navigation Office (CSNO) (2017a) BeiDou navigation satellite system signal in space interface control document open service signal B1C (Version 1.0). Available online: P02017a1226741342013031.pdf (beidou.gov.cn)

China Satellite Navigation Office (CSNO) (2017b) BeiDou navigation satellite system signal in space interface control document open service signal B2a (Version 1.0). Available online: P02017b1226742357364174.pdf (beidou.gov.cn)

China Satellite Navigation Office (CSNO) (2021) BeiDou navigation satellite system open service performance standard (Version 3.0). Available online: http://www.beidou.gov.cn/xt/gfxz/202105/P020210526216231136238.pdf

Deng Y, Guo F, Ren X, Ma F, Zhang X (2021) Estimation and analysis of multi-GNSS observable-specific code biases. GPS Solut 25(3):1–13. https://doi.org/10.1007/s10291-021-01139-6

Desai SD (2002) Observing the pole tide with satellite altimetry. J Geophys Res Oceans 107(C11):7-1–7-13. https://doi.org/10.1029/2001JC001224

Dilner F, Seeber G, Schmitz Wübbena G, Tosos G, Maeusli D (2006) Characterisation of GOCE SSTI antennas. Zeitschrift für Geodäsie. Geoinf Und Landmanag (zfv) 131:61–71

Enge P (2003) GPS modernization: capabilities of the new civil signals. Australian international aerospace congress, Brisbane, 29 July-1 August 2003

Folkner WM, Williams JG, Boggs DH (2014) The planetary and lunar ephemerides DE430 and DE431. Interplanet Netw Prog Rep 196(1):42–196. https://doi.org/10.3847/1538-3881/abd414

Gambis D (2004) Monitoring earth orientation using space-geodetic techniques: state-of-the-art and prospective. J Geod 78(4/5):295–303. https://doi.org/10.1007/s00190-004-0394-1

Guo J, Xu X, Zhao Q, Liu J (2016) Precise orbit determination for quad-constellation satellites at Wuhan University: strategy, result validation, and comparison. J Geod 90(2):143–159. https://doi.org/10.1007/s00190-015-0862-9

Haines B, Bar-Sever Y, Bertiger W, Desai S, Willis P (2004) One-centimeter orbit determination for Jason-1: new GPS based strategies. Mar Geod 27(1–2):299–318. https://doi.org/10.1080/01490410490465300

Hauschild A, Montenbruck O, Sleewaegen JM, Huisman L, Teunissen PJG (2012) Characterization of compass M-1 signals. GPS Solut 16(1):117–126. https://doi.org/10.1007/s10291-011-0210-3

Jäggi A, Hugentobler U, Bock H, Beutler G (2007) Precise orbit determination for GRACE using undifferenced or doubly differenced GPS data. Adv Space Res 39(10):1612–1619. https://doi.org/10.1016/j.asr.2007.03.012

Jäggi A, Dach R, Montenbruck O, Hugentobler U, Bock H, Beutler G (2009) Phase center modeling for LEO GPS receiver antennas and its impact on precise orbit determination. J Geod 83(12):1145. https://doi.org/10.1007/s00190-009-0333-2

Jiao WH et al (2011) Monitoring and assessment of GNSS Open Services (in Chinese). Sci Sin Phys Mech Astron 41:521–527. https://doi.org/10.1360/132011-359

Jin B, Li Y, Jiang K, Li Z, Chen S (2021) GRACE-FO antenna phase center modeling and precise orbit determination with single receiver ambiguity resolution. Remote Sens 13(21):4204. https://doi.org/10.3390/rs13214204

Kang Z, Nagel P, Pastor R (2003) Precise orbit determination for GRACE. Adv Space Res 31(8):1875–1881. https://doi.org/10.1016/S0273-1177(03)00159-5

Kroes R, Montenbruck O, Bertiger W, Visser P (2005) Precise GRACE baseline determination using GPS. GPS Solutions 9(1):21–31. https://doi.org/10.1007/s10291-004-0123-5

Li M, Li W, Shi C, Jiang K, Guo X, Dai X, Meng X, Yan Z, Yang G, Liao M (2017) Precise orbit determination of the Fengyun-3C satellite using onboard GPS and BDS observations. J Geod 91(11):1313–1327. https://doi.org/10.1007/s00190-017-1027-9
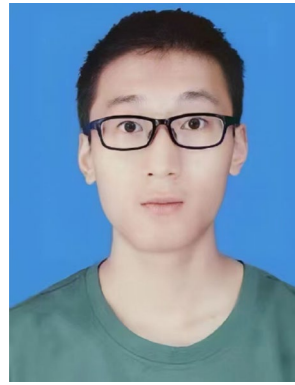
Li X, Ma T, Xie W, Zhang K, Huang J, Ren X (2019) FY-3D and FY-3C onboard observations for differential code biases estimation. GPS Solut 23(2):1–14. https://doi.org/10.1007/s10291-019-0850-2

Loyer S, Perosanz F, Mercier F, Capdeville H, Marty J (2012) Zero-difference GPS ambiguity resolution at CNES–CLS IGS analysis center. J Geod 86(11):991–1003. https://doi.org/10.1007/s00190-012-0559-2

Lu M, Li W, Yao Z, Cui X (2019) Overview of BDS III new signals. NAVIG J Inst Navig 66(1):19–35. https://doi.org/10.1002/navi.296

Luzum B, Petit G (2012) The IERS Conventions (2010): reference systems and new models. Proc Int Astron Union 10(H16):227–228. https://doi.org/10.1017/S1743921314005535

Lyard F, Lefevre F, Letellier T, Francis O (2006) Modelling the global ocean tides: modern insights from FES2004. Ocean Dyn 56(5–6):394–415. https://doi.org/10.1007/s10236-006-0086-x

Männel B, Deng Z, Ge M, Sakic P, Nischan T, Brandt A, Bradke M, Ramatschi M (2017) GFZ analysis center technical report 2017. IGS Central Bureau, 54

Marshall JA, Luthcke SB (1994) Modeling radiation forces acting on TOPEX/Poseidon for precision orbit determination. J Spacecr Rocket 31(1):99–105. https://doi.org/10.2514/3.26408

Montenbruck O, Kroes R (2003) In-flight performance analysis of the CHAMP BlackJack GPS receiver. GPS Solutions 7(2):74–86. https://doi.org/10.1007/s10291-003-0055-5

Montenbruck O, Van Helleputte T, Kroes R, Gill E (2005) Reduced dynamic orbit determination using GPS code and carrier measurements. Aerosp Sci Technol 9(3):261–271. https://doi.org/10.1016/j.ast.2005.01.003

Montenbruck O et al (2008) Tracking and orbit determination performance of the GRAS instrument on MetOp-A. GPS Solut 12(1):289–299. https://doi.org/10.1007/s10291-008-0091-2

Montenbruck O, Garcia-Fernandez M, Yoon Y, Schön S, Jäggi A (2009) Antenna phase center calibration for precise positioning of LEO satellites. GPS Solut 13(1):23. https://doi.org/10.1007/s10291-008-0094-z

Montenbruck O et al (2017) The Multi-GNSS Experiment (MGEX) of the International GNSS Service (IGS)–achievements, prospects and challenges. Adv Space Res 59(7):1671–1697. https://doi.org/10.1016/j.asr.2017.01.011

Montenbruck O, Hackel S, Jäggi A (2018) Precise orbit determination of the Sentinel-3A altimetry satellite using ambiguity-fixed GPS carrier phase observations. J Geod 92(7):711–726. https://doi.org/10.1007/s00190-017-1090-2

Montenbruck O, Steigenberger P, Hauschild A (2020) Comparing the 'Big 4'-A user's view on GNSS performance. 2020 IEEE/ION position, location and navigation symposium (PLANS). IEEE 2020:407–418. https://doi.org/10.1109/PLANS46316.2020.9110208

Montenbruck O, Hackel S, Wermuth M, Zangerl F (2021) Sentinel-6A precise orbit determination using a combined GPS/Galileo receiver. J Geod 95(109):1–17. https://doi.org/10.1007/s00190-021-01563-z

Mu R, Dang Y, Xu C (2020) BDS-3/GNSS data quality and positioning performance analysis. China Satellite Navigation Conference. Springer, Singapore, 368–379. https://doi.org/10.1007/978-981-15-3707-3_35

NSOAS (2022) HY-2: a marine remote sensing satellite series planned by China. http://www.nsoas.org.cn/index.html

Odijk D, Zhang B, Teunissen P J G (2015) Multi-GNSS PPP and PPP-RTK: some GPS+ BDS results in Australia. China satellite navigation conference (CSNC) 2015 proceedings: volume II. Springer, Berlin, Heidelberg, pp 613-623. https://doi.org/10.1007/978-3-662-46635-3_52

Pavlis E C, Luceri V, Sciarretta C, Kelm R (2020) The ILRS contribution to ITRF2008. University of Maryland at Baltimore County Faculty Collection.

Peng H, Jiang K, Li M, Wang Y, Wang X, Fang R, Lin M, Zhao Q (2021) Single-Differenced Ambiguity Resolution for Orbit Determination of the Haiyang-2B. IEEE J Sel Top Appl Earth Obs Remote Sens 14:7121–7132. https://doi.org/10.1109/JSTARS.2021.3097082

Petit G, Luzum B (2010) IERS conventions (2010) Bureau International des Poids et mesures sevres (france). https://doi.org/10.1038/138755d0

Rocken C, Meertens C (1992) UNAVCO receiver tests. UNAVCO Memo, Nov 8, 1992

Sanz J, Miguel Juan J, Rovira-Garcia A, González-Casado G (2017) GPS differential code biases determination: methodology and analysis. GPS Solut 21(4):1549–1561

Shako R, et al (2014) EIGEN-6C: a high-resolution global gravity combination model including GOCE data. Observation of the system earth from space-CHAMP, GRACE, GOCE and future missions, pp 155–161

Shi C, Wu X, Zheng F, Wang X, Wang J (2021) Modeling of BDS-2/BDS-3 single-frequency PPP with B1I and B1C signals and positioning performance analysis. Measurement 178:109355. https://doi.org/10.1016/j.measurement.2021.109355

Tranquilla JM, Carr JP (1990) GPS multipath field observations at land and water sites. Navigation 37(4):393–414. https://doi.org/10.1002/j.2161-4296.1990.tb01564.x

Van J, den Ijssel J, Visser P, Patiño E, Rodriguez, (2013) Champ precise orbit determination using GPS data. Adv Space Res 31(8):1889–1895. https://doi.org/10.1016/S0273-1177(03)00161-3

Villiger A, Schaer S, Dach R, Prange L, Sušnik A, Jäggi A (2019) Determination of GNSS pseudo-absolute code biases and their long-term combination. J Geod 93(9):1487–1500. https://doi.org/10.1007/s00190-019-01262-w

Wang E, Yang T, Wang Z, Zhang Y, Guo J, Shu W, Qu P (2021) Performance evaluation of precise point positioning for BeiDou-3 B1c/B2a signals in the global range. Sensors 21(17):5780. https://doi.org/10.3390/s21175780

Wang Y, Li M, Jiang K, Li W, Zhao Q, Peng H, Lin M (2022) Precise orbit determination of the Haiyang 2C altimetry satellite using attitude modeling. GPS Solut 26(1):1–14. https://doi.org/10.1007/s10291-021-01219-7

Yang Y, Mao Y, Sun B (2020) Basic performance and future developments of BeiDou global navigation satellite system. Satell Navig 1(1):1–8. https://doi.org/10.1186/s43020-019-0006-0

Zhao Q, Wang C, Guo J, Yang G, Liao M, Ma H, Liu J (2017) Enhanced orbit determination for BeiDou satellites with FengYun-3C onboard GNSS data. GPS Solut 21(3):1179–1190. https://doi.org/10.1007/s10291-017-0604-y

Zhao X, Zhou S, Ci Y, Hu X, Cao J, Chang Z, Tang C, Guo D, Guo K, Liao M (2020) High-precision orbit determination for a LEO nanosatellite using BDS-3. GPS Solut 24(4):1–14. https://doi.org/10.1007/s10291-020-01015-9

Zhao Q (2004) Research on precision orbit determination theory and software of both GPS navigation constellation and LEO Satellites. Dissertation, Wuhan University. https://doi.org/10.3321/j.issn:1671-8860.2005.04.029

Min Li received a B.S. degree and Ph.D. degree in Geodesy and Surveying Engineering from Wuhan University, Wuhan, China, in 2005 and 2011, respectively. He was a Research Fellow with the Hong Kong Polytechnic University and is currently a professor at GNSS Research Center of Wuhan University. His main work focuses on GNSS satellite orbit determination and precise point positioning as well as multi-GNSS processing using GPS, GLONASS, BeiDou, and Galileo.

Renhai Mu received an M.S. degree from the Chinese Academy of Surveying & Mapping, Beijing, China, in 2021 and is currently working toward a doctoral degree with Wuhan University, Wuhan, China. His main research interests include the precise orbit determination of low earth spacecraft and dynamics model refinement.

Kecai Jiang is currently a postdoctor at the GNSS Research Center of Wuhan University. He received a Ph.D. from Wuhan University in 2020 and is currently a postdoctoral researcher at Wuhan University. His current research mainly focuses on LEO and side lobe signal HEO orbit determination using GNSS.

Youcun Wang received an M.S. degree in Geomatics Engineering from Shandong University of Science and Technology, Qingdao, China, in 2019. He is currently working toward a doctoral degree at Wuhan University, Wuhan, China. His main research interests include the precision orbit determination of LEO and dynamics model refinement.

Xuanxuan Zhang obtained his bachelor's degree at the China University of Geosciences, Beijing, and is a master's student at the Chinese Academy of Surveying and Mapping. His main interest is in GNSS high-precision data processing.

Chuntao Chang obtained his bachelor's degree at the Shandong University of Technology in 2017 and is currently a master's candidate at the Chinese Academy of Surveying and mapping. CGCS2000 framework maintenance and GNSS high-precision data processing are his main research interest.

Qile Zhao received a Ph.D. degree from Wuhan University, Wuhan, China, in 2004 and an M.S. degree from the Institute of Geology, China Earthquake Administration, Wuhan, China, in 1998. In 2006–2007, as a postdoctoral fellow, he did his postdoctoral program in DEOS, Delft University of Technology, the Netherlands. He is currently a professor at the GNSS Research Center of Wuhan University, and His current research interests are precise orbit determination of GNSS and low earth orbit satellites and high-precision positioning using GPS, Galileo, and BeiDou systems.